

Semimetal Contacts to Monolayer Semiconductor: Weak Metalization as an Effective Mechanism to Schottky Barrier Lowering

Tong Su,^{1,2,3} Yueyan Li,^{4,5} Qianqian Wang,³ Weiwei Zhao,^{1,2} Liemao Cao,^{6,*} and Yee Sin Ang^{3,†}

¹*Savage Laboratory for Smart Materials, School of Materials Science and Engineering,
Harbin Institute of Technology, Shenzhen 518055, China*

²*Shenzhen Key Laboratory of Flexible Printed Electronics Technology,
Harbin Institute of Technology, Shenzhen 518055, China*

³*Science, Mathematics and Technology, Singapore University of Technology and Design, Singapore 487372*

⁴*School of Information Management, Nanjing University, Nanjing 210023, China*

⁵*Jiangsu Key Laboratory of Data Engineering and Knowledge Service, Nanjing 210023, China*

⁶*College of Physics and Electronic Engineering, Hengyang Normal University, Hengyang 421002, China*

Recent experiment has uncovered semimetal bismuth (Bi) as an excellent electrical contact to monolayer MoS₂ with ultralow contact resistance. The contact physics of the broader semimetal/monolayer-semiconductor family beyond Bi/MoS₂, however, remains largely unexplored thus far. Here we perform a comprehensive first-principle density functional theory investigation on the electrical contact properties between six archetypal two-dimensional (2D) transition metal dichalcogenide (TMDC) semiconductors, i.e. MoS₂, WS₂, MoSe₂, WSe₂, MoTe₂ and WTe₂, and two representative types of semimetals, Bi and antimony (Sb). As Bi and Sb work functions energetically aligns well with the TMDC conduction band edge, Ohmic or nearly-Ohmic *n*-type contacts are prevalent. The interlayer distance of semimetal/TMDC contacts are significantly larger than that of the metal/TMDC counterparts, which results in only weak metalization of TMDC upon contact formation. Intriguingly, such weak metalization generates semimetal-induced gap states (MIGS) that extends below the conduction band minimum, thus offering an effective mechanism to reduce or eliminate the *n*-type Schottky barrier height (SBH) while still preserving the electronic structures of 2D TMDC. A modified Schottky-Mott rule that takes into account SMIGS, interface dipole potential, and Fermi level shifting is proposed, which provides an improved agreement with the DFT-simulated SBH. We further show that the tunneling-specific resistivity of Sb/TMDC contacts are generally lower than the Bi counterparts, thus indicating a better charge injection efficiency can be achieved through Sb contacts. Our findings reveal the promising potential of Bi and Sb as excellent companion electrode materials for advancing 2D semiconductor device technology.

I. INTRODUCTION

Two-dimensional (2D) semiconductors offer an exciting material platform for extending the legacy of Moore's law beyond silicon [1–3]. Their ultimately-thin body enables excellent electrostatic control of the channel, which, when combined with the exceptional electrical properties, provides a route towards ultrascaled sub-10-nm field-effect transistor (FET) technology that are promising in delivering a future generation of computing electronics with simultaneous high performance and ultralow energy consumption. The path towards high-performance 2D semiconductor devices is, however, severely impeded by multiple technical roadblocks [4, 5]. In particular, the design and fabrication of high-efficiency Ohmic contact to 2D semiconductor represents one of the major challenges [6, 7]. The search of a CMOS compatible Ohmic contact engineering approach remains an ongoing challenge thus far.

Recently, semimetal electrodes, such as bismuth (Bi), antimony (Sb) and tin (Sn), emerge as an excellent contact candidate materials to transition metal dichalco-

genide (TMDC) monolayer semiconductor with an experimentally demonstrated low Schottky barrier height (SBH), low contact resistance (R_c) and high on-state current (I_{on}) [8–11]. R_c as low as 123 $\Omega\mu\text{m}$ has been achieved in Bi/MoS₂ contact, with a sizable on-state current density of $I_{on} \sim 10^3 \mu\text{A}/\mu\text{m}$. Semimetals thus represent a promising CMOS-compatible strategy in resolving the contact engineering challenges of 2D semiconductor devices, which is in contrast to the van der Waals (vdW) 2D and 3D contact engineering approaches that typically involve stringent fabrication processes not readily compatible with the mainstream CMOS technology [12–14]. Instead of relying on weak interfacial coupling to tame the Fermi level pinning (FLP) effect – an undesirable effect that pins the Fermi level (ε_F) of an electrode to the midgap region of a semiconductor [15] which leads to an undesirably high contact barrier that cannot be easily reduced [16–18] – as in the case of 2D and 3D vdW contacts [19–24], the limited availability of states around the Fermi level (ε_F) in semimetallic Bi intrinsically quenches FLP upon contact formation. The weakened FLP enables the ε_F of Bi to be more freely align to the conduction band minima (CBM) of MoS₂, thus achieving Ohmic or nearly Ohmic contacts with ultralow contact resistance. Recent demonstrations of dual-gated Bi/WS₂ FET device geometry [25, 26] show that R_c can be improved by nearly 20 times via contact gating while mul-

* Email: liemao.cao@hynu.edu.cn

† Email: yeemin.ang@sutd.edu.sg

TABLE I. **Summary of DFT calculated physical quantities of the 12 types of semimetal/TMDC contacts.** E_b is the binding energy, ϵ is the lattice mismatch, d is the perpendicular interlayer distance, $\epsilon_F^{(\text{iso})}$ is the Fermi level of the isolated semimetal after receiving a strain arising from lattice mismatch, $\epsilon_F^{(\text{sm/sc})}$ is the Fermi level of the contact heterostructure, E_{EA} is the electron affinity, E_{IP} is the ionization potential, $\Phi_{\text{SBH}}^{(e)}$ is the electron (n -type) Schottky barrier height, ΔV is the interface potential difference, Δ_M is the weak metalization energy window below conduction band edge, $\Delta\epsilon_F$ is the Fermi level shifting of the semimetal upon forming contact heterostructures, Φ_t is the van der Waals gap tunneling potential height and w_t is the width of the tunneling potential width. The unstrained isolated Bi and Sb slabs have a Fermi level of -4.12 eV and -4.25 eV, respectively, below the vacuum layer. The stacking configurations are quoted in the format of ‘semimetal super cell, TMDC supercell’. All energy-related quantities (E_b , $\epsilon_F^{(\text{iso})}$, $\epsilon_F^{(\text{sm/sc})}$, E_{EA} , E_{IP} , $\Phi_{\text{SBH}}^{(e)}$, ΔV , Δ_M , $\Delta\epsilon_F$ and Φ_t) are in the unit of (eV) and all length-related quantities (d and w_t) are in the unit of \AA .

Heterostructures	E_b	ϵ (%)	Stacking	d	$\epsilon_F^{(\text{iso})}$	$\epsilon_F^{(\text{sm/sc})}$	E_{EA}	E_{IP}	$\Phi_{\text{SBH}}^{(e)}$	ΔV	Δ_M	$\Delta\epsilon_F$	Φ_t	w_t
MoS ₂ /Bi	-2.41	3.8	2×2, 3×3	2.94	-4.33	-4.45	-4.33	-5.99	0.08	0.17	0.05	0.21	2.80	1.26
WS ₂ /Bi	-2.22	3.8	2×2, 3×3	3.03	-4.33	-4.29	-3.95	-5.75	0.13	0.03	0.22	0.21	2.97	1.33
MoSe ₂ /Bi	-1.49	4.6	2×2, $\sqrt{7}\times\sqrt{7}$	3.08	-3.86	-4.03	-3.95	-5.42	-0.09	-0.15	0.16	-0.26	2.68	1.30
WSe ₂ /Bi	-1.42	4.6	2×2, $\sqrt{7}\times\sqrt{7}$	3.15	-3.86	-3.88	-3.62	-5.23	-0.09	-0.02	0.35	-0.26	2.75	1.42
MoTe ₂ /Bi	-2.36	2.2	2×2, $\sqrt{7}\times\sqrt{7}$	3.14	-4.31	-4.24	-3.87	-4.90	0.00	0.21	0.37	0.19	2.58	1.26
WTe ₂ /Bi	-2.24	2.0	2×2, $\sqrt{7}\times\sqrt{7}$	3.21	-4.30	-4.23	-3.66	-4.71	0.04	0.33	0.54	0.18	2.65	1.26
MoS ₂ /Sb	-1.03	3.8	2×2, $\sqrt{7}\times\sqrt{7}$	3.08	-4.00	-4.34	-4.34	-6.02	-0.08	-0.29	0.08	-0.25	3.09	1.47
WS ₂ /Sb	-0.98	3.8	2×2, $\sqrt{7}\times\sqrt{7}$	3.21	-4.00	-4.12	-3.94	-5.76	-0.06	-0.08	0.24	-0.24	3.15	1.50
MoSe ₂ /Sb	-1.51	3.8	2×2, $\sqrt{7}\times\sqrt{7}$	3.07	-4.38	-4.32	-3.95	-5.37	-0.06	0.10	0.43	0.13	2.96	1.33
WSe ₂ /Sb	-1.45	3.8	2×2, $\sqrt{7}\times\sqrt{7}$	3.16	-4.38	-4.31	-3.62	-5.04	0.06	0.21	0.63	0.13	3.14	1.41
MoTe ₂ /Sb	-4.00	2.5	3×3, $\sqrt{13}\times\sqrt{13}$	3.26	-4.10	-4.13	-3.87	-4.86	-0.04	0.15	0.30	-0.15	2.73	1.27
WTe ₂ /Sb	-3.91	2.7	3×3, $\sqrt{13}\times\sqrt{13}$	3.32	-4.09	-4.11	-3.66	-4.69	-0.03	0.24	0.48	-0.16	2.82	1.35

tiscale modelling predicts an exceedingly low $R_c < 100 \Omega\mu\text{m}$ when the doping level of TMDC and an appropriate dielectric environment are chosen [27]. These results suggest the availability of multiple tuning knobs that can be used to further optimize the contact resistance, thus unravelling the enormous potential of semimetal-based 2D semiconductor device technology [28].

Although spearheading experimental efforts focusing on several semimetal/monolayer-TMDC contacts have shed important light on the device level performance of semimetal contacts, the interfacial electronic properties and contact formation at the microscopic physics level, which are important for device design and computational modelling, remains largely incomplete thus far. Whether semimetals can be employed to the broader family of 2D TMDC for achieving efficient contacts remains an open research question that needs to be urgently answered before the full potential of semimetal contact engineering can be fully harnessed.

In this work, we carry out first-principle density functional theory (DFT) investigations that comprehensively covers 12 species of semimetal/semiconductor contact heterostructures composed of transition metal dichalcogenide (TMDC) monolayers MX_2 ($M = \text{Mo}, \text{W}; X = \text{S}, \text{Se}, \text{Te}$) [29] and semimetals Bi and Sb. We show that n -type Ohmic and nearly Ohmic contacts with ultralow Schottky barrier height (SBH) prevail among the 12 contact heterostructures due to the presence of weak metalization ‘tail’ states that extend below the CBM [30]. The weak metalization induced by Bi and Sb thus pro-

vides an effective mechanism to achieve efficient Ohmic contact engineering for TMDC monolayers without introducing severe FLP effect. A modified Schottky-Mott relation with inclusion of (i) interface dipole correction; (ii) Fermi level offset of semimetal upon contact formation; and (iii) a hybridization term characterizing the degree of hybridization between semimetals and monolayer semiconductors is proposed, which provides an improved agreement with the observed SBH when compared to the original Schottky-Mott relation. We further show that Sb is a potentially superior semimetal contact due to their generally lower tunneling-specific resistivity than that of the Bi counterparts. Our findings provide practical insights on the electronic structures and contact properties of semimetal/2D-TMDC contact heterostructures, and shall pave a foundation for the computational design and the experimental exploration of high-performance low-power 2D semiconductor devices based on semimetal electrical contacts.

II. COMPUTATIONAL METHODS

First-principle calculations are performed with the Vienna ab initio simulation package (VASP) with projector augmented wave method [31–34]. The exchange-correlation interaction with the generalized gradient approximation (GGA) of Perdew, Burke and Ernzerhof (PBE) [35] is set and the DFT-D3 [36] vdW better describe the interlayer vdw interaction. A kinetic energy

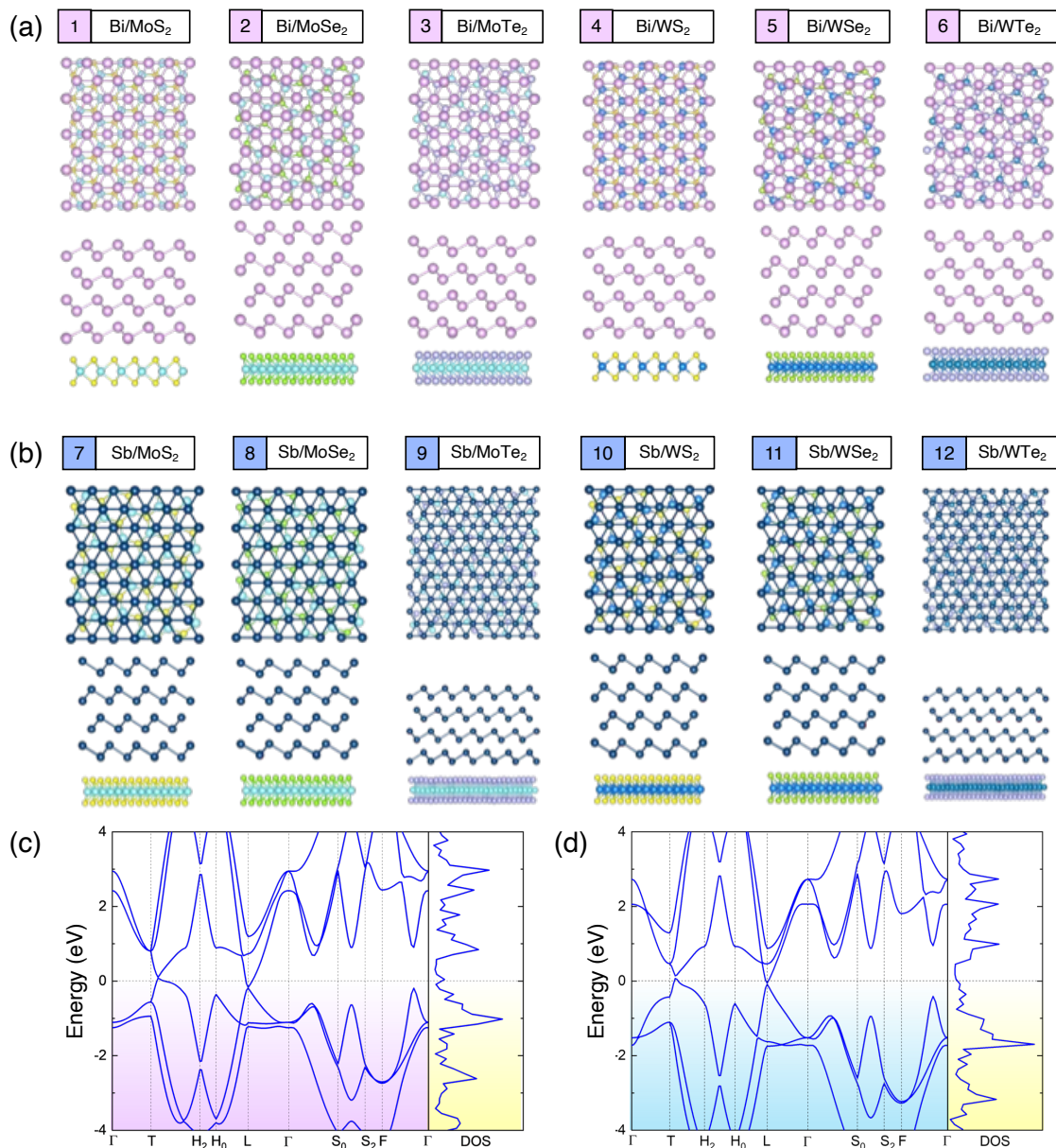


FIG. 1. **Stacking configurations of semimetal contacts to monolayer transition metal dichalcogenide (TMDC) and band structures of semimetals.** (a) Stacking configurations of bismuth-contacted monolayer TMDC. (b) Same as (a) but with antimony (Sb) contact. (c) and (d) show the band structures and electronic density of states of isolated Bi and Sb bulk.

cutoff of 500 eV to make the plane expansion meet the 10^{-2} eV/Å force and 10^{-6} eV energy convergence criteria. A fine Monkhorst-Pack k-sampling is set in the gamma-centered Brillouin zone with $6 \times 6 \times 1$. We apply a vacuum spacing of at least 15 Å to the heterostructure. Dipole corrections are applied due to the symmetry-breaking nature of the contact heterostructures [37].

III. RESULTS AND DISCUSSION

A. Structural and Lattice structures

The stacking configurations of the Bi and Sb contacts to TMDC monolayers are shown in Fig. 1(a) and 1(b), respectively. We employ the combinations of 2×2 Bi with 3×3 (Mo,W)S₂, and 3×3 Sb with $\sqrt{13} \times \sqrt{13}$ (Mo,W)Te₂, while the rest of the contact heterostructures are all based on 2×2 semimetal combined $\sqrt{7} \times \sqrt{7}$ TMDC monolayer (see Table I for summary of the stack-

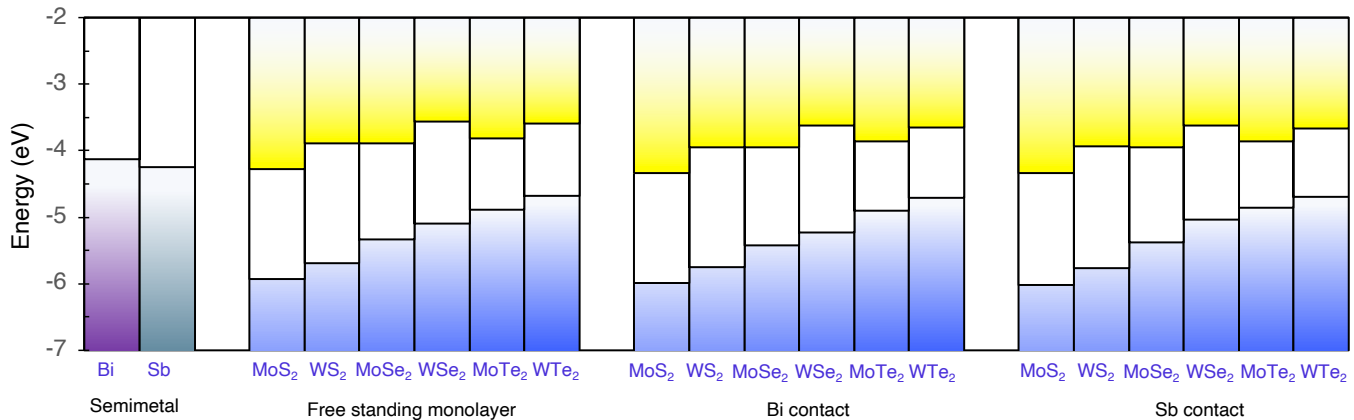


FIG. 2. **Band alignment of semimetals, monolayer TMDCs and the semimetal-contacted TMDCs.** The Fermi level of semimetals and the band edge energies of the monolayer TMDCs are measured with respect to vacuum level.

ing configurations and other calculated quantities). Four layers of Bi or Sb atoms are used to simulate the bulk semimetal contacts. The lattice mismatch lies within the range of 2% to 4.6%, and the strains are applied to the semimetals so to preserve the electronic band structures of monolayer TMDCs. The fully relaxed interlayer distance of the contacts are typically $> 3 \text{ \AA}$, which is significantly larger than those of the electrical contacts between 3D metals and TMDC monolayer [38–40]. Such sizable interlayer distance spatially decouple the semimetals and the monolayer TMDC, thus leads to a diminished metalization between semimetal and monolayer TMDC. The binding energies of the heterostructures are calculated as

$$E_b = E_{sm/sc} - E_{sm} - E_{sc} \quad (1)$$

where $E_{sm/sc}$, E_{sm} and E_{sc} are the total energy per supercell of the contact heterostructure, the semimetal and the semiconductor, respectively. The negative-valued E_b of all heterostructures indicate that the contact formation is energetically favourable (see Table I). The band structure of bulk Bi and Sb are shown in Figs. 1(c) and 1(d). The conduction and valence bands lightly touch or overlap near the Fermi level at L point and along the T - H_2 axis, thus yielding the semimetallic nature.

B. Electronic properties: Band structure and interfacial electron redistribution

The band alignment of TMDC monolayers and the ε_F of Sb and Bi are shown in Fig. 2. The ε_F of Bi and Sb (i.e. 4.12 eV and 4.25 eV below the vacuum level, respectively) aligns at the close proximity of the CBM of monolayer TMDC (~ 4 eV). Such band alignment thus suggests monolayer TMDC to form n -type Schottky or Ohmic contacts with Bi and Sb semimetals. However, it should be noted that the Anderson rule cannot be directly applied to determine the contact types due to the presence of interfacial charge transfer and orbital

hybridization effect that could significantly modify the band edge energies and the overall band alignment of the contact heterostructures [41]. This aspect is particularly evident from the electronic band structures of the semimetal contacts shown in Fig. 2. Here although the ε_F of Bi and Sb are energetically separated from the CBM of TMDC other than (Mo,W)S₂ monolayers by a sizable 0.2 ~ 0.7 eV, Ohmic or nearly Ohmic contacts are still prevalent among these semimetal-contacted TMDC monolayers. As shown below, the presence of weak metalization in semimetal-contacted TMDC is highly beneficial in lowering the SBH and transfers the contacts towards Ohmic or low-SBH contacts.

A closer inspection on the projected band structures and the projected density of states (PDOS) reveals that the Ohmic contact formations in semimetal-contacted TMDC monolayers arises from the weak metalization induced by Bi and Sb upon contact formation. The presence of weak metalization on TMDC creates semimetal-induced gap states (SMIGS) that extend below the CBM energies of TMDC monolayers, thus closing up the energy mismatch, i.e. SBH, between the semimetal and the monolayer TMDC. Weak metalization thus offer a mechanism to lower the SBH while still preserving the semiconducting band edge states of monolayer TMDC. Low SBH is particularly beneficial for thermionic and tunneling charge injection [42, 43] into monolayer TMDC, thus paving a way to achieve ultralow contact resistance in 2D semiconductor devices. We further note that the DFT-calculated SBHs of Bi/MoS₂ (0.075 eV) and Bi/WS₂ (0.13 eV) differ from the experimentally extracted zero-height (i.e. Ohmic) of Bi/MoS₂ and 0.040 eV of Bi/WS₂. We suspect that such discrepancy could arise from the inevitable presence of defects at the contacted region in experiment which leads to stronger metalization and more extensive SMIGS in monolayer TMDC that lower the SBH of the contacts. Nevertheless, the general trend of Bi/WS₂ having a larger SBH than Bi/MoS₂ obtained via DFT calculations is agreement with that observed experimentally.

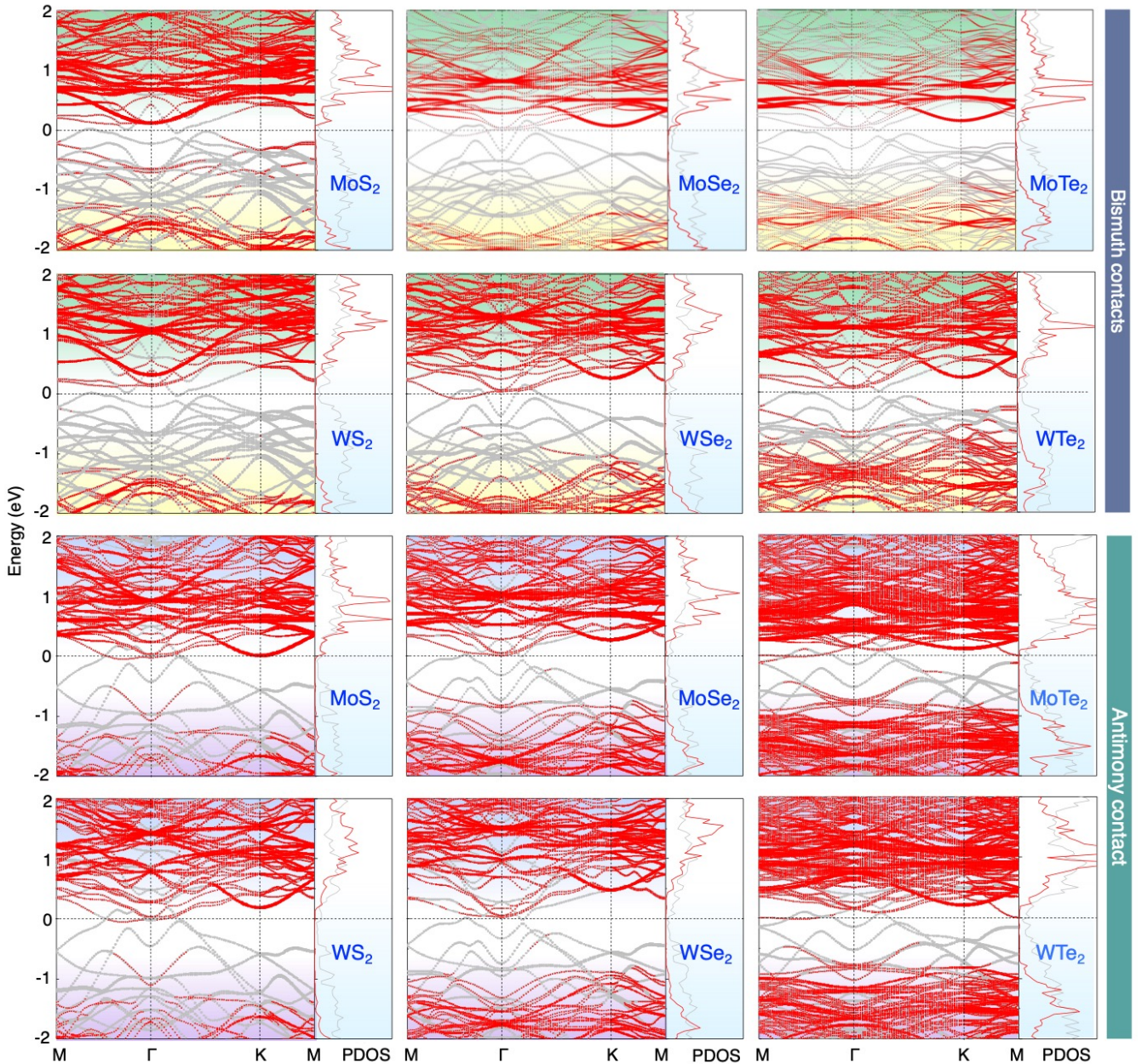


FIG. 3. **Band structures of semimetal-contacted monolayer TMDC.** The band structures are projected onto semimetal (grey) and monolayer semiconductor (red). The projected density of states (PDOS) are shown in the left panel of each band structure plots.

The electron redistribution and the interfacial potential difference reveal great wealth of contact physics and interfacial interactions of metal/semiconductor heterostructures [44–46]. The electron redistribution across the contact interface can be assessed via the differential charge density of the heterostructures ($\Delta\rho$), which is can be calculated as

$$\Delta\rho = \rho_{\text{sm/sc}} - \rho_{\text{sm}} - \rho_{\text{sc}} \quad (2)$$

where $\rho_{\text{sm/sc}}$, ρ_{sm} and ρ_{sc} are the electron densities of the contact heterostructure, semimetal and semiconduc-

tor, respectively. Electron redistribution across the interface results in the formation of an interface potential difference, i.e.

$$\Delta V = W_{\text{sm/sc}}^{(\text{sm})} - W_{\text{sc/sc}}^{(\text{sc})} \quad (3)$$

where $W_{\text{sm/sc}}^{(\text{sc})}$ and $W_{\text{sc/sc}}^{(\text{sc})}$ are the work functions extracted from the semiconductor and the semimetal sides of the contact heterostructure, respectively.

The $\Delta\rho$ and ΔV are shown in Fig. 4. We observe complex electron redistribution patterns across the contact interfaces from the $\Delta\rho$ plots (see left and middle

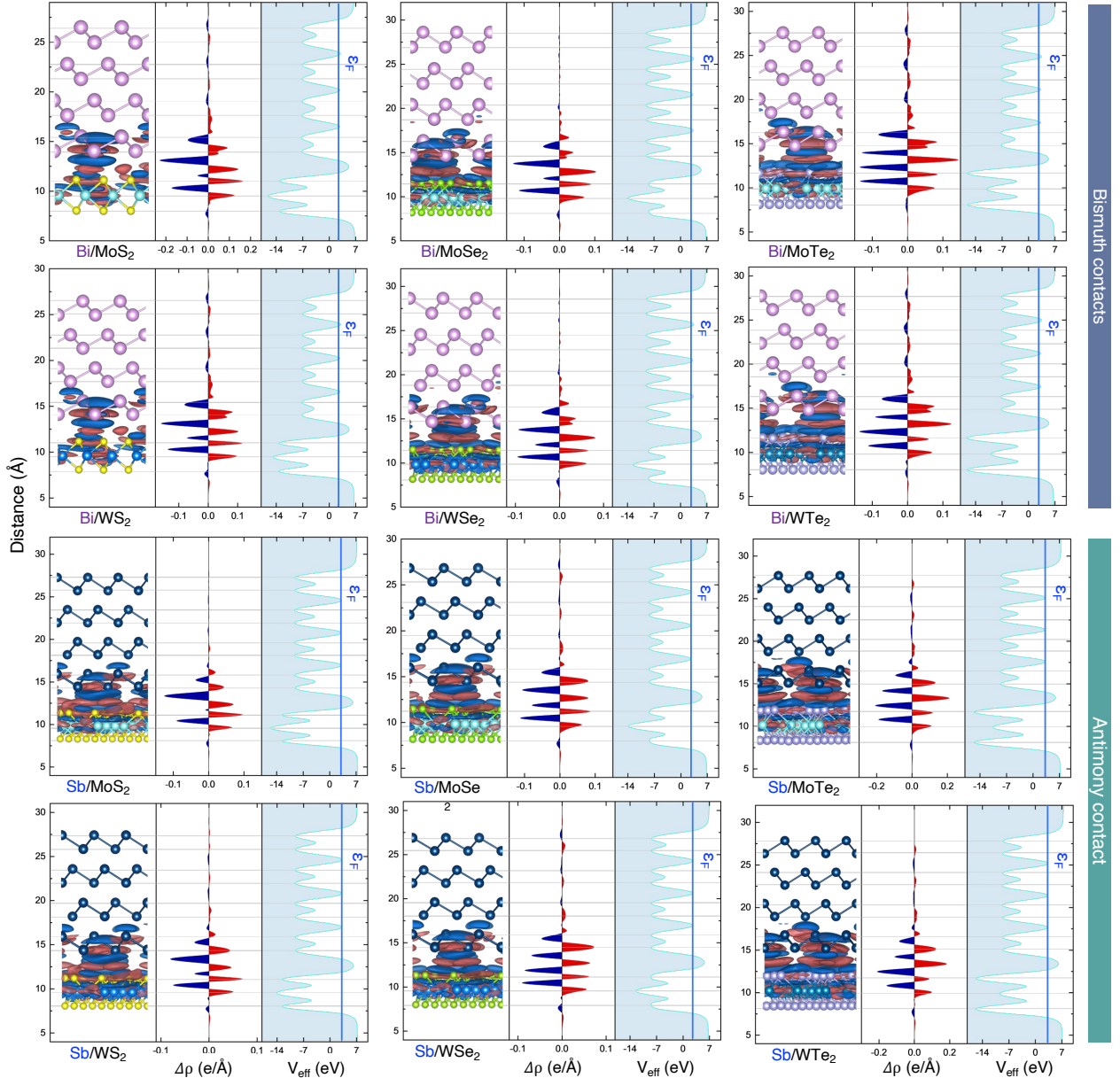


FIG. 4. **Charge transfer and electrostatic potential profile of the semimetal/TMDC contacts.** The differential charge density distribution plotted onto the lattice (left panel), the plane-averaged differential charge density plots (middle panel) and the plane-averaged electrostatic potential profiles (right panel) are shown for Bi- and Sb-contacted TMDC monolayers.

panels of Fig. 4), in which electron accumulation (depletion) are denoted by red (blue) isosurfaces and red (blue) shaded curves. Charge redistribution occurs through the entire thickness of TMDC due to the weak screening effect of 2D semiconductor, which is in stark contrast to that of semimetals in which electron redistribution effect are rapidly screened and does not penetrate beyond the outermost layer of Bi or Sb atoms. In general, electrons accumulate on both (i) the outermost contacting layer of the semimetals; and (ii) the chalcogen atoms at the contact interface. These electron accumulations arise from different physical origins. The electron accumulation on

the semimetal atoms is due to the electronic pushback (or ‘pillow’) effect [44, 45]. In this case, electrons are pushed back towards the semimetal so to minimize the wavefunction overlap, and hence the Pauli exchange repulsion, between the semimetal and the chalcogen atoms at the contact interface. This results in electron accumulation on the semimetal sides of the contact interface. The electron accumulation on the chalcogen atoms occurs due to their stronger electronegativity nature when compared with the semimetal atoms. The stronger electronegativity of the chalcogen atoms causes a net displacement of electron densities towards TMDC, thus leading to electron

accumulation on the chalcogen atoms. Correspondingly, whether the resulting dipole potential ΔV is positive or negative-valued depends on the ‘tug-of-war’ between the electronic pushback effect and the electronegativity difference of semimetal and chalcogen atoms. Contact with stronger electronic pushback effect exhibits a positive valued ΔV , and is indicative of physisorptive interfacial interaction [45]. In contrast, if the electron transfer due to electronegativity difference dominates over the electronic pushback effect, a negative valued ΔV is obtained, which is indicative of chemisorptive interfacial interaction [45]. For semimetal/2D-TMDC contacts, the ΔV ranges from -0.29 to 0.33 eV, thus suggesting that both chemisorption and physisorption can occur upon contact formation.

We define the electronegativity difference ($\Delta\chi$) as

$$\Delta\chi = \chi_{\text{chalcogen}} - \chi_{\text{semimetal}} \quad (4)$$

where $\chi_{\text{chalcogen}}$ and $\chi_{\text{semimetal}}$ are the electronegativity of the chalcogen and semimetal atoms, respectively. Here $\chi_{\text{S,Se,Te}} = (2.58, 2.55, 2.1)$, respectively, and $\chi_{\text{Bi,Sb}} = (2.02, 2.05)$, respectively. Contacts with small $\Delta\chi$ exhibits positive-valued ΔV [see Fig. 5(a) for a plot of ΔV versus $\Delta\chi$] due to the dominance of electronic pushback effect which leads to overall charge accumulation on the semimetal. The interfacial interaction of semimetal-contacted Te-based TMDC, which has small $\Delta\chi$, is thus dominated by the electronic pushback effect, and the contacts fall under the physisorption type with weaker interfacial coupling effect. In contrast, contacts with large $\Delta\chi$ tends to exhibit low or negative valued ΔV [Fig. 5(a)] due to the stronger overall electron density shifting towards the TMDC side. Here the interface couples strongly, thus resulting in the chemisorption contact types in S- and Se-based TMDC upon contacted by semimetals. The physisorption of Te-based TMDC and chemisorption of S- and Se-based TMDC on semimetals are also evident from the semimetal-TMDC interlayer distance (d) [Fig. 5(b)]. Contacts with smaller d tends to have lower or negative-valued ΔV which is consistent with chemisorptive interfacial interaction that binds the two materials more strongly, while contacts with larger d tends to have larger or positive-valued ΔV which is indicative of physisorptive interfacial interaction in which electronic pushback effect dominates.

It should be noted that the physisorption and chemisorption effect are also observed in metal/2D-TMDC contact heterostructures, such as the physisorptive Pt/MoS₂ [46] which preserves the electronic structures of TMDC, and the chemisorptive Ti/MoS₂ [45], In/MoS₂ [47] and W/MoS₂ [48] in which the TMDC is severely metalized. In contrast, semimetal/2D-TMDC contact exhibits only mild metalization when compared to that of the metal counterparts [49] (see band structure and PDOS plots in Fig. 3.) This aspect thus represents a major distinction between metal and semimetal contacts to 2D TMDCs.

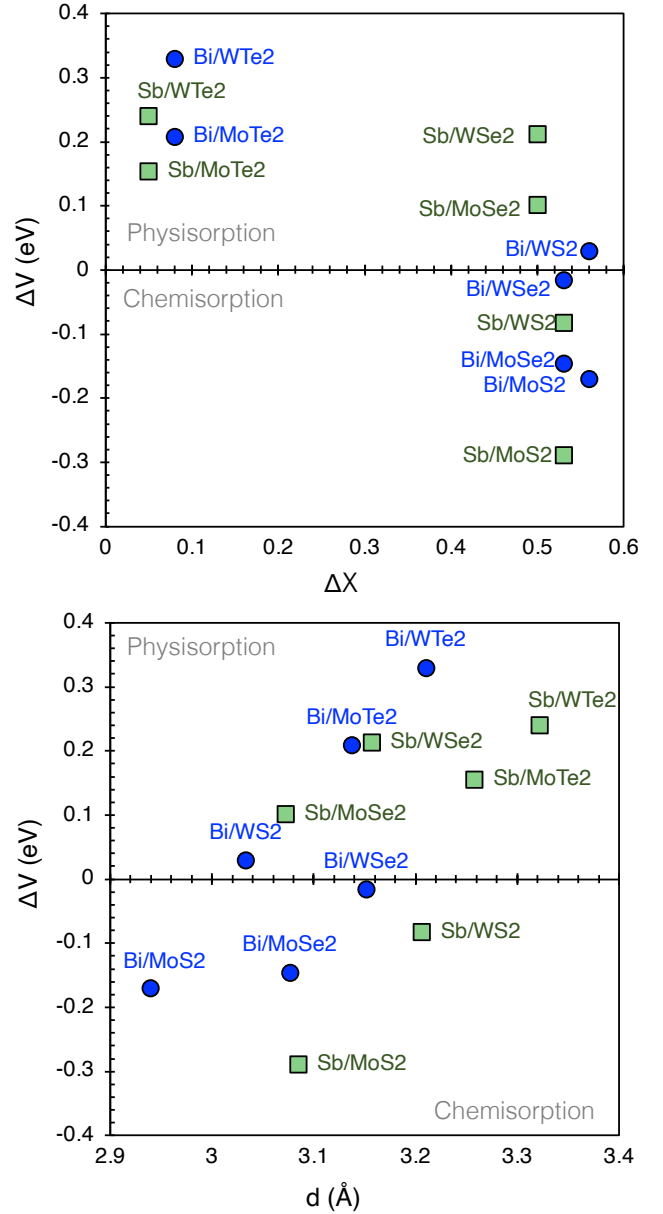


FIG. 5. **Interface dipole potential (ΔV) of semimetal/TMDC contacts.** (a) ΔV as a function of the electronegativity difference $\Delta\chi$. (b) ΔV as a function of the interlayer distance d .

C. Metalization effect and van der Waals contact

We now investigate the metalization effect on TMDC upon forming contact with semimetals. Taking Bi/MoSe₂ as a representative contact, the band-decomposed charge density [see Figs. 6(a) and 6(b)] of the CBM states and within the energy window of Δ_M below the CBM which contains the SMIGS as one can directly see from the band structure and PDOS plots in Fig. 3. For CBM states, the charge density spatially distributes in both TMDC and semimetal. As ΔH

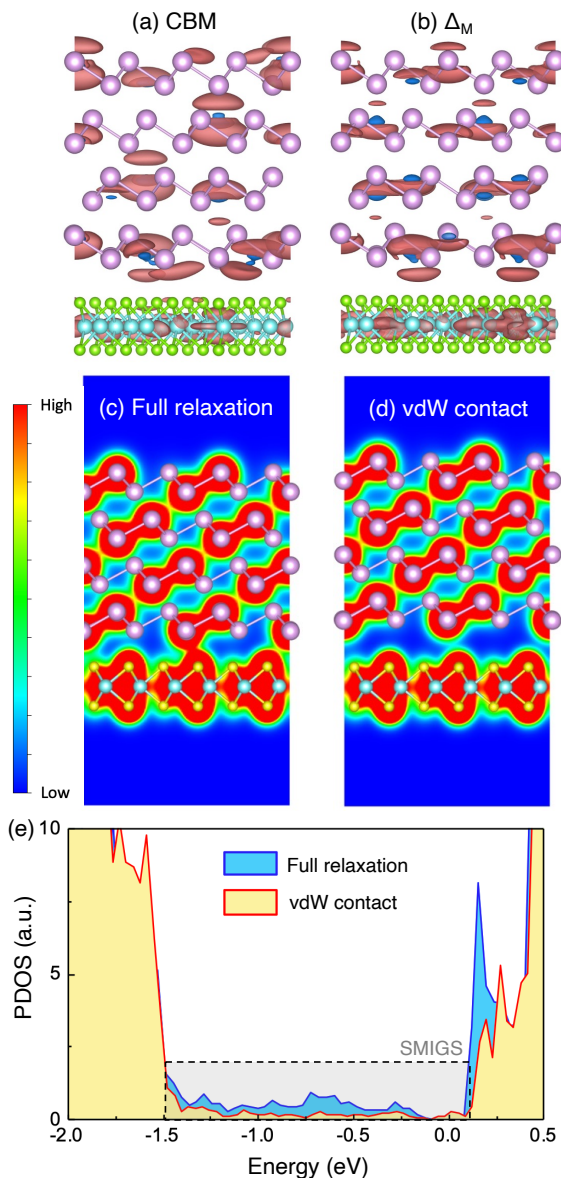


FIG. 6. **Metalization and van der Waals contacts in semimetal/TMDC heterostructures.** (a) The band-decomposed charge density plot of CBM states in Bi/MoSe₂ contact. (b) Same as (a) but for the energy range of Δ_M below the CBM. (c) Charge density plot of fully relaxed Bi/MoSe₂ with interlayer distance of 2.94 Å, and (d) with vdW distance 3.86 Å. (e) Electronic density of states projected on to MoS₂ monolayer for fully relaxed and vdW contacts.

lies in the band gap regime of TMDC, the charge density should only concentrate on the semimetals but not on the TMDC in the case of an ideal non-interacting semimetal/TMDC contact interface. This is, however, not the case in a realistic contact, such as the illustrative example of Bi/MoSe₂ shown in Figs. 6(b). Here the charge density distribution of the electronic states lying within the ΔH energy window extends well into MoSe₂, thus indicating the presence of metalization effect.

The metalization of TMDC can be suppressed by spatially separating the two contacting materials to reduce the interfacial interactions. In fact, such strategy has been employed in metal/TMDC contact via the formation of atomically clean and weakly coupled vdW contacts [19–21, 50] which offers an effective way to suppress FLP and to achieve ultralow contact resistance. We compare the contact properties of a fully-relaxed Bi/MoSe₂ heterostructure with an interlayer distance d (see Table I) and that of a Bi/MoSe₂ contact constructed using vdW gap distance (d_{vdW}) [51],

$$d_{\text{vdW}} = r_{\text{vdW}}^{(\text{Bi})} + r_{\text{vdW}}^{(\text{S})} \quad (5)$$

where $r_{\text{vdW}}^{(\text{Bi})} = 2.07$ Å and $r_{\text{vdW}}^{(\text{S})} = 1.87$ Å are the vdW radii of Bi and S atoms, respectively. At the fully-relaxed interlayer distance d , the electronic orbitals of Bi overlap with that of the S atoms [see Fig. 6(c)]. Such orbital overlap is significantly reduced in the case of vdW contact [Fig. 6(d)]. The presence of SMIGS in MoS₂ upon contacted by Bi can be clearly observed in the PDOS in Fig. 6(e). In the case of vdW contact, the SMIGS are significantly suppressed. Because of the suppression of the SMIGS in vdW contacts, the PDOS of MoS₂ terminates sharply below the CBM. This results in a larger SBH in vdW-type Bi/MoSe₂ contact, thus suggesting that vdW contact may not be ideal for applications where SBH are required to be minimized.

D. Modified Schottky-Mott theory and tunneling-specific resistivity

For a non-interacting ideal metal/semiconductor contact, the electron SBH ($\Phi_{\text{SBH}}^{(e)}$) of an n -type Schottky contact is given by the Schottky-Mott (SM) rule [52],

$$\Phi_{\text{SBH}}^{(e)} = W_{\text{metal}} - E_{\text{EA}} \quad (6)$$

where W_{metal} and E_{EA} are the isolated metal work function and the electron affinity of the isolated semiconductor. The ideal SM rule, however, omits the metal-semiconductor interfacial interactions which are inevitable in almost all realistic contact heterostructures [53, 54]. For 2D-metal/2D-semiconductor contact, the presence of an interfacial potential difference (ΔV) induced by charge redistribution generates an additional band offset term [55] that modifies the SBH. Accordingly, the SM rule is modified as [56–58]

$$\Phi_{\text{SBH}}^{(e)} = W_{\text{metal}} - E_{\text{EA}} - \Delta V \quad (7)$$

where a positive ΔV , i.e. electron accumulation on 2D metal, increases the metal work function and lowers the electron SBH. In 3D-metal/2D-semiconductor contact, the presence of significant interfacial interaction further complicates the SBH formation physics [59]. For example, in Au-contacted MoS₂, an intermediate recon-

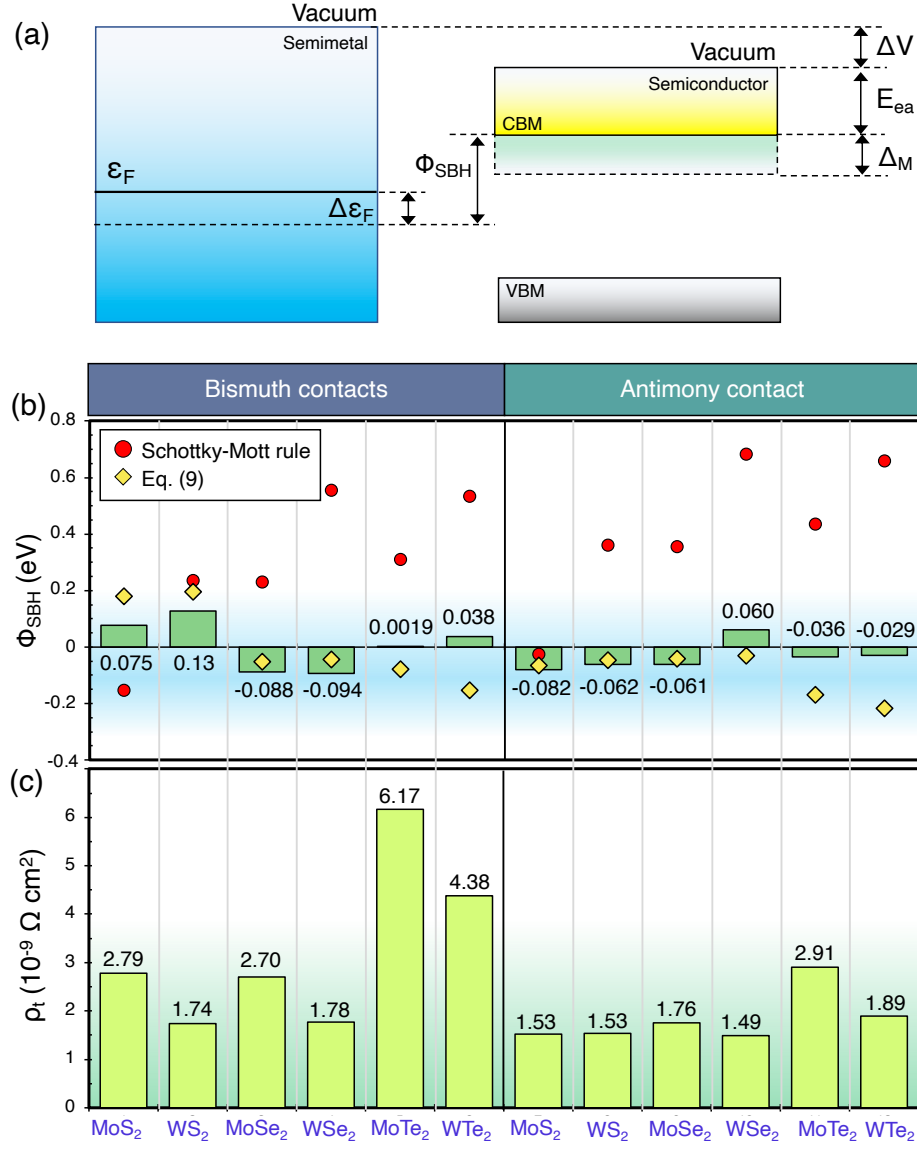


FIG. 7. **Schottky barrier heights (SBH) and tunneling-specific contact resistivity (ρ_t) of semimetal/TMDC contacts.** (a) Schematic drawing of the modified Schottky-Mott (SM) rule that takes into account SMIGS (Δ_M), interface dipole potential (ΔV) and Fermi level shifting ($\Delta\epsilon_F$) of the semimetal. (b) SBH extracted from the DFT calculated band structure and PDOS (vertical bars), and the predicted SBH values of SM rule [Eq. (6)] and of modified SM rule [Eq. (9)]. (c) Tunneling-specific contact resistivity calculated based on Simmons tunneling diode model.

structured Au₄S₄ layer can form at the Au/MoS₂ interface, which modifies the SM rule by an additional quasi-bonding correction term that accounts for the formation of electronic tail states extending from the band edges induced by quasi-bonding (QB) effect [60]. The presence of QB-induced gap states (QBIGS) modifies the SM rule to

$$\Phi_{SBH}^{(e)} = W_{\text{metal}} - E_{EA} - \Delta V - \Delta_{QB} \quad (8)$$

where Δ_{QB} is the energy window of the QBIGS. Motivated by the formulation of Eq. (8), we propose a modi-

fied SM rule for semimetal/2D-TMDC contacts, i.e.

$$\Phi_{SBH}^{(e)} = W_{\text{metal}} - E_{EA} - \Delta V + \Delta\epsilon_F - \Delta_M \quad (9)$$

where $\Delta\epsilon_F \equiv \epsilon_F^{(\text{sm/sc})} - \epsilon_F^{(\text{iso})}$ is the Fermi level shifting upon contact formation which arises due to lattice mismatch when constructing the heterostructure supercell, and Δ_M is the energy window of the SMIGS. In Fig. 6(a), we compare the electron SBH extracted from PDOS, the predicted SBH from the SM rule in Eq. (6), and that from the modified SM rule in Eq. (9). We find that while the original SM rule fails to predict the SBH of almost all contacts, the modified SM rule exhibits a significantly improved agreement with the DFT calculation results [Fig.

7(a)]. This observation thus highlights the importance of both interface potential difference and SMIGS in the formation of SBH in semimetal/2D-TMDC contacts.

The presence of a vdW gap at the contact interface yields a potential barrier through which the electrons must tunnel across in order to form an injection current into the monolayer TMDC. The corresponding *tunneling-specific contact resistivity* [8, 38, 39] can be computed based on the Simmons tunneling diode model for a square potential barrier [61], i.e.

$$\rho_t \approx \frac{4\pi^2 \hbar w_t^2 \exp\left(\frac{2\sqrt{2m}}{\hbar} w_t \phi_t^{1/2}\right)}{e^2 \frac{\sqrt{2m}}{\hbar} w_t \phi_t^{1/2} - 1} \quad (10)$$

where ϕ_t and w_t are the vdW gap tunneling barrier height and width measured with respect to the Fermi level, respectively, which can be extracted from the plane-average electrostatic plots across the contact heterostructures (i.e. Fig. 4) [62]. The calculated ρ_t [Fig. 7(b)] are generally in the order of $10^{-9} \Omega\text{cm}^2$, which is similar to that of Bi/MoS₂ [8] and other 2D semiconductor metal contacts, such as MoSi₂N₄ [38] and γ -GeSe [39] monolayers. The Te-based TMDC generally exhibit larger ρ_t than other TMDC monolayers due to the physisorptive contact interface with larger interlayer distance, which generates a wider tunneling barrier to suppresses electron tunneling. We further observe that the Sb/2D-TMDC contacts generally exhibits lower ρ_t when compared to that of the Bi counterparts. The lower ρ_t and better thermal stability [9] of Sb compared to Bi contacts suggests that Sb contact shall serve as an efficient semimetal contact materials for 2D TMDC.

IV. CONCLUSION

In conclusion, we performed a first-principle density functional theory simulation to investigate the contact properties between Bi and Sb semimetal to monolayer

TMDCs. We found that weak metalization generates semimetal-induced gap states (SMGIS) that are beneficial in lowering the Schottky barrier height (SBH), thus offering a pathway to achieve Ohmic or low-barrier contacts without compromising the semiconductor electronic band structures. The physisorptive and chemisorptive nature of the various contacts are identified. A modified Schottky-Mott (SM) rule that takes into account interface dipole potential and SMGIS are found to improve the theoretical description of SBH over the original SM rule. Finally, the contact-specific resistivity of Sb contacts are found to be generally lower than Bi contacts, thus unravelling the potential of Sb-contacted monolayer TMDC for energy-efficient device application. These findings shall offer a theoretical foundation and design blueprint for the future exploration of semimetal-enabled high-performance 2D semiconductor nanoelectronics and novel devices, such as valleytronics [63, 64] and multiferroics [65, 66].

DATA AVAILABILITY STATEMENT

The data that support the findings of this study are available upon reasonable request from the authors.

ACKNOWLEDGEMENT

This work is funded by the Singapore Ministry of Education (MOE) Academic Research Fund (AcRF) Tier 2 Grant (MOE-T2EP50221-0019) and SUTD-ZJU IDEA Visiting Professor Grant (SUTD-ZJU (VP) 202001). T. S. is supported by the China Scholarship Council (CSC). W. Z. is supported by the Natural Science Foundation of China (No. 52073075) and Shenzhen Science and Technology Program (Grant No. KQTD20170809110344233). The computational work for this article was partially performed on resources of the National Supercomputing Centre, Singapore (<https://www.nsc.sg>).

-
- [1] Pal A, Zhang S, Chavan T, Agashiwala K, Yeh CH, Cao W and Banerjee K 2022 Quantum-Engineered Devices Based on 2D Materials for Next-Generation *Adv. Mater.* n/a 2109894
 - [2] Huang X, Liu C, and Zhou P 2022 2D semiconductors for specific electronic applications: from device to system *NPJ 2D Mater. Appl.* 6 51
 - [3] Akinwande D, Huyghebaert C, Wang CH, Serna MI, Goossens S, Li LJ, Wong HP and Koppens FH 2019 Graphene and two-dimensional materials for silicon technology *Nat.* 573 507
 - [4] Schram T, Sutar S, Radu I, and Asselberghs I 2022 Challenges of Wafer-Scale Integration of 2D Semiconductors for High-Performance Transistor Circuits *Adv. Mater.* n/a 2109796
 - [5] Thomas S 2021 An industry view on two-dimensional materials in electronics *Nat. Electron.* 4 856
 - [6] Zheng Y, Gao J, Han C and Chen W 2021 Ohmic Contact Engineering for Two-Dimensional Materials *Cell Reports Physical Science* 2 100398
 - [7] Ang YS, Cao L and Ang LK 2021 Physics of electron emission and injection in two-dimensional materials: Theory and simulation *InfoMat.* 3 502
 - [8] Shen PC, Su C, Lin Y, Chou AS, Cheng CC, Park JH, Park JH, Chiu MH, Lu AY, Tang HL, Tavakoli MM, Pitner G, Ji X, Cai Z, Mao N, Wang J, Tung V, Li J, Bokor J, Zettl A, Wu CI, Palacios T, Li LJ and Kong J 2021 Ultralow contact resistance between semimetal and monolayer semiconductors *Nat.* 593 211
 - [9] Chou AS, Wu T, Cheng CC, Zhan SS, Ni IC, Wang SY, Chang YC, Liew SL, Chen E, Chang WH, Wu CI, Cai

- J, Wong HSP and Wang H 2021 Antimony Semimetal Contact with Enhanced Thermal Stability for High Performance 2D Electronics *IEDM* 7
- [10] Chou AS, Cheng CC, Liew SL, Ho PH, Wang SY, Chang YC, Chang CK, Su YC, Huang ZD, Fu YF, Hsu CK, Chung YY, Chang WH and Li LJ 2020 High on-state current in chemical vapor deposited monolayer MoS_2 nFETs with Sn ohmic contacts *IEEE ELECTR DEVICE L* 42 272
- [11] Cao Z, Lin F, Gong G, Chen H and Martin J 2020 Low Schottky barrier contacts to $2H - MoS_2$ by Sn electrodes *Appl. Phys. Lett.* 116 022101
- [12] Pham PV, Bodepudi SC, Shehzad K, Liu Y, Xu Y, Yu B and Duan X 2022 2D Heterostructures for Ubiquitous Electronics and Optoelectronics: Principles, Opportunities, and Challenges *Chem. Rev.* 122 6514
- [13] Liu Y, Huang Y and Duan X 2019 Van der Waals integration before and beyond two-dimensional materials *Nat.* 567 323
- [14] Zheng Y, Gao J, Han C and Chen W 2021 Ohmic contact engineering for two-dimensional materials *Cell Reports Physical Science* 2 100298
- [15] Bardeen J 1947 Surface States and Rectification at a Metal-Semiconductor Contact *Phys Rev.* 71 717
- [16] Kim C, Moon I, Lee D, Choi MS, Ahmed F, Nam S, Cho Y, Shin HJ, Park S and Yoo WJ 2017 Fermi level pinning at electrical metal contacts of monolayer molybdenum dichalcogenides *ACS nano.* 11 1588
- [17] Gong C, Colombo L, Wallace RM and Cho K 2014 The unusual mechanism of partial Fermi level pinning at metal- MoS_2 interfaces *Nano Lett.* 14 1714
- [18] Liu X, Choi MS, Hwang E, Yoo WJ and Sun J 2022 Fermi Level Pinning Dependent 2D Semiconductor Devices: Challenges and Prospects *Adv. Mater.* 34 2108425
- [19] Liu Y, Stradins P and Wei SH 2016 Van der Waals metal-semiconductor junction: Weak Fermi level pinning enables effective tuning of Schottky barrier *Sci. adv.* 2 e1600069
- [20] Liu Y, Guo J, Zhu E, Liao L, Lee SJ, Ding M, Shakir I, Gambin V, Huang Y and Duan XF 2018 Approaching the Schottky-Mott limit in van der Waals metal-semiconductor junctions *Nat.* 557 696
- [21] Wang Y, Kim JC, Wu RJ, Martinez J, Song X, Yang J, Zhao F, Mkhoyan A, Jeong HY and Chhowalla M 2019 Van der Waals contacts between three-dimensional metals and two-dimensional semiconductors *Nat.* 568 70
- [22] Huang T, Chen Q, Cheng MQ, Huang WQ, Hu W and Huang GF 2019 Tunable Schottky barrier in van der Waals heterostructures of graphene and hydrogenated phosphorus carbide monolayer: first-principles calculations *J. Phys. D* 52 305104
- [23] Yu JQ, Ke SS and Lü HF 2021 Electronic properties and tunable Schottky barrier of non-Janus *J. Phys. D* 55 035104
- [24] Jiang B, Yang Z, Liu X, Liu Y and Liao L 2019 Interface engineering for two-dimensional semiconductor transistors *Nano Today* 25 122
- [25] Jin L and Koester SJ 2022 Contact Gating in Dual-Gated WS_2 MOSFETs With Semi-Metallic Bi Contacts *IEEE ELECTR DEVICE L* 43 1575
- [26] Jin L and Koester SJ 2022 High-Performance Dual-Gated Single-Layer WS_2 MOSFETs With Bi Contacts *IEEE ELECTR DEVICE L* 43 639
- [27] Wu T and Guo J 2022 Multiscale modeling of semimetal contact to two-dimensional transition metal dichalcogenide semiconductor *Appl. Phys. Lett.* 121 023507
- [28] Quhe R, Xu L, Liu S, Yang C, Wang Y, Li H, Yang J, Li Q, Shi B, Li Y, Pan Y, Sun X, Li J, Weng M, Zhang H, Guo Y, Xu L, Tang H, Dong J, Yang J, Zhang Z, Lei M, Pan F, Lu J 2021 Sub-10 nm two-dimensional transistors: theory and experiment *Phys. Rep.* 938 1
- [29] Jariwala D, Sangwan VK, Lauhon LJ, Marks TJ and Hersam MC 2014 Emerging device applications for semiconducting two-dimensional transition metal dichalcogenides *ACS nano.* 8 1102
- [30] Kang J, Liu W, Sarkar D, Jena D and Banerjee K 2014 Computational Study of Metal Contacts to Monolayer Transition-Metal Dichalcogenide Semiconductors *Phys. Rev. X* 4 031005
- [31] Kresse G and Hafner J 1993 Ab initio molecular dynamics for liquid metals *Phys. Rev. B* 47 558
- [32] Kresse G and Furthmüller J 1996 Efficiency of ab-initio total energy calculations for metals and semiconductors using a plane-wave basis set *Comp. Mater. Sci.* 6 15
- [33] Blöchl PE 1994 Projector augmented-wave method *Phys. Rev. B* 50 17953
- [34] Kresse G and Joubert D 1999 From ultrasoft pseudopotentials to the projector augmented-wave method *Phys. Rev. B* 59 1758
- [35] Perdew JP, Burke K and Ernzerhof M 1996 Generalized gradient approximation made simple *Phys. Rev. Lett.* 77 3865
- [36] Grimme S, Antony J, Ehrlich S and Krieg H 2010 A consistent and accurate ab initio parametrization of density functional dispersion correction (DFT-D) for the 94 elements H-Pu *J. Chem. Phys.* 132 154104
- [37] Neugebauer J and Scheffler M 1992 Adsorbate-substrate and adsorbate-adsorbate interactions of Na and K adlayers on Al (111) *Phys. Rev. B* 46 16067
- [38] Wang Q, Cao L, Liang SJ, Wu W, Wang G, Lee CH, Wee LO, Yang HY, Ang LK, Yang SY 2021 Efficient Ohmic contacts and built-in atomic sublayer protection in $MoSi_2N_4$ and WSi_2N_4 monolayers *NPJ 2D Mater. Appl.* 5 71
- [39] Cao L, Deng X, Tang Z, Zhou G and Ang YS 2022 Designing high-efficiency metal and semimetal contacts to two-dimensional semiconductor Γ -GeSe *Appl. Phys. Lett.* 121 113104
- [40] Tang H, Shi B, Pan Y, Li J, Zhang X, Yan J, Xu L, Yang J, Wu M and Lu J 2019 Schottky Contact in Monolayer WS_2 Field-Effect Transistors *Adv. Theory Simul.* 2 1900001
- [41] Besse R, Silveira JFRV, Jiang Z, West D, Zhang S and Da Silva, JLF 2021 Beyond the Anderson rule: importance of interfacial dipole and hybridization in van der Waals heterostructures *2D Mater.* 8 041002
- [42] Somvanshi D, Kallatt S, Venkatesh C, Nair S, Gupta G, Anthony JK, Karmakar D and Majumdar K 2017 Nature of carrier injection in metal/2D-semiconductor interface and its implications for the limits of contact resistance *Phys. Rev. B* 96 205423
- [43] Ang YS, Yang HY and Ang LK 2018 Universal scaling laws in Schottky heterostructures based on two-dimensional materials *Phys. Rev. Lett.* 121 056802
- [44] Bokdam M, Brocks G and Kelly PJ 2014 Large potential steps at weakly interacting metal-insulator interfaces *Phys. Rev. B* 90 201411

- [45] Farmanbar M and Brocks G 2016 First-principles study of van der Waals interactions and lattice mismatch at MoS₂/metal interfaces *Phys. Rev. B* 93 085304
- [46] Wang Q, Shao Y and Shi X 2020 Mechanism of charge redistribution at the metal–semiconductor and semiconductor–semiconductor interfaces of metal–bilayer MoS₂ junctions *J. Chem. Phys.* 152 244701
- [47] Kim BK, Kim TH, Choi DH, Kim H, Watanabe K, Taniguchi T, Rho H, Kim JJ, Kim YH and Bae MH 2021 Origins of genuine Ohmic van der Waals contact between indium and MoS₂ *NPJ 2D Mater. Appl.* 5 9
- [48] Gao J and Gupta M 20 Titanium disulfide as Schottky/ohmic contact for monolayer molybdenum disulfide *NPJ 2D Mater. Appl.* 4 26
- [49] Chen Y, Li Y, Wu J and Duan W 2017 General criterion to distinguish between Schottky and Ohmic contacts at the metal/two-dimensional semiconductor interface *Nanoscale* 9 2068
- [50] Liu K, Luo P, Han W, Yang S, Zhou S, Li H and Zhai T 2019 Approaching ohmic contact to two-dimensional semiconductors *Sci. Bull.* 64 1426
- [51] Kwon G, Choi YH, Lee H, Kim HS, Jeong J, Jeong K, Baik M, Kwon H, Ahn J, Lee E and Cho MH 2022 Interaction-and defect-free van der Waals contacts between metals and two-dimensional semiconductors 5 241
- [52] Tung RT 2014 The physics and chemistry of the Schottky barrier height *Appl. Phys. Rev.* 1 011304
- [53] Tung RT and Kronik L 2021 Quantitative explanation of the Schottky barrier height *Phys. Rev. B* 103 035304
- [54] Kong L, Zhang X, Tao Q, Zhang M, Dang W, Li Z, Feng L, Liao L, Duan X and Liu Y 2020 Doping-free complementary WSe₂ circuit via van der Waals metal integration *Nat. Commun.* 11 1866
- [55] Tung RT and Kronik L 2018 Charge Density and Band Offsets at Heterovalent Semiconductor Interfaces *Adv. Theory Simul.* 1 1700001
- [56] Si C, Lin Z, Zhou J and Sun Z 2016 Controllable Schottky barrier in GaSe/graphene heterostructure: the role of interface dipole *2D Mater.* 4 015027
- [57] Ding X, Zhao Y, Xiao H and Qiao L 2021 Engineering Schottky-to-ohmic contact transition for 2D metal–semiconductor junctions *Appl. Phys. Lett.* 118 091601
- [58] Li J, Zhou W, Xu L, Yang J, Qu H, Guo T, Xu B, Zhang, S and Zeng H 2022 *Mater. Today Phys.* 26 100749
- [59] Allain A, Kang J, Banerjee K and Kis A 2015 Electrical contacts to two-dimensional semiconductors *Nat. Mater.* 14 1195
- [60] Zhou LX, Ren YT, Chen YT, Lv XH, Jin CD, Zhang H, Gong PL, Lian RQ, Wang RN, Wang JL and Shi XQ 2022 Quasi-bonding-induced gap states in metal/two-dimensional semiconductor junctions: Route for Schottky barrier height reduction *Phys. Rev. B* 105 224105
- [61] Simmons JG 1963 Generalized Formula for the Electric Tunnel Effect between Similar Electrodes Separated by a Thin Insulating Film *J. Appl. Phys.* 34 1793
- [62] Wang Y, Liu S, Li Q, Quhe R, Yang C, Guo Y, Zhang X, Pan Y, Li J, Zhang H, Xu L, Shi B, Tang H, Li Y, Zhang Z, Xiao L, Pan F and Lu J 2021 Schottky barrier heights in two-dimensional field-effect transistors: from theory to experiment *Rep. Prog. Phys.* 84 056501
- [63] Zhang T, Xu X, Huang B, Dai Y, Kou L and Ma Y 2023 Layer-polarized anomalous Hall effects in valleytronic van der Waals bilayers *Mater. Horiz.* DOI: 10.1039/D2MH00906D
- [64] Ang YS, Yang SA, Zhang C, Ma Z and Ang LK 2017 Valleytronics in merging Dirac cones: All-electric-controlled valley filter, valve, and universal reversible logic gate *Phys. Rev. B* 96 245410
- [65] Zhang T, Liang Y, Xu X, Huang B, Dai Y and Ma Y 2021 Ferroelastic-ferroelectric multiferroics in a bilayer lattice *Phys. Rev. B* 103 165420
- [66] Cao L, Deng X, Zhou G, Liang S-J, Nguyen CV, Ang LK and Ang YS 2022 Multiferroic van der Waals heterostructure FeCl₂/Sc₂CO₂: Nonvolatile electrically switchable electronic and spintronic properties *Phys. Rev. B* 105 165302